ACCEPTED PAPER

Characterization of RF-driven atmospheric pressure Ar plasma micro-jet plume

Davood Hassanpour , Seyyed-Jalal Pestehe*

Advanced Plasma Laboratory, Faculty of Physics, University of Tabriz, Tabriz, Iran

Corresponding author: sjpest@yahoo.com

Characterization of RF-Driven Atmospheric Pressure Ar Plasma Micro-jet Plume

Davood Hassanpour , Seyyed-Jalal Pestehe*

Advanced Plasma Laboratory, Faculty of Physics, University of Tabriz

davood_hp@yahoo.com , sjpest@yahoo.com

Abstract

The plasma parameters of an RF-driven plasma microjet in different applied RF powers, different positions from the outlet nozzle, and various argon flow rates are investigated. A double Langmuir probe is designed and constructed, then, the electron temperature, ion density, and saturation currents along the microjet axis at different positions such as top, mid, end and out of the microjet are measured. To avoid the collision, sparking, and corrosion effects, in high pressure plasmas, on the characteristic curve, the double Langmuir probe was reciprocated linearly perpendicular to the plasma jet with a frequency of 20 Hz. The four frequently used methods of the direct fitting of the theoretically obtained formula, double slope, turning point or Dote, and cutting or intercept method are explained and used to determine the electron excitation temperature from the experimental data and shown that they lead to similar results, so, the averaged value of these results used in the evaluations of plasma densities. The plasma number density and electron temperature were measured using DLP in the jet at different axial locations. The results for the electron excitation temperature from the DLP is compared with that of obtained from the emission spectrum of the plasma jet. It has been shown that the averaged electron excitation temperature obtained using optical emission spectroscopy ($1.58eV$) is within the 25% of that measured by the double Langmuir probe which is same as the early reported value by other researches.

Keywords: Atmospheric pressure cold plasma microjet, Langmuir double probe, RF microjet, electron temperature, plasma density, Optical emission spectroscopy

1. Introduction

The use of the atmospheric pressure plasma jets (APPJs) is in the focus of scientists, craftsmen and physicians because of their low gas temperatures $(\sim 300\text{-}1000\,\text{K})$ [1], capability of producing different active species such as neutral metastable species and radicals as well as (V)UV radiation. The importance of these sources in biomedical applications, such as deactivation of bacteria on heat sensitive surfaces, wound healing or cancer treatment are well known [2,3,4,5,6,7,8]. The investigations on the device geometry [9,10], characteristics of the produced plasmas [11] and its interaction with the surface of the living and non-living materials are still open in research [2,12,13,14]. Therefore completing the human knowledge on any of these subjects is extremely important.

Considering geometrical aspects of view, one can find a large number of different APPJ designs driven with different power sources including DC, AC, RF, MW as well as pulsed voltages in different frequencies [3,6,9,12,15,16,17]. However, the control of plasma parameters and properties such as temperature, electron/ion density and fluxes, as well as reactive species densities, energies and lifetimes is still a key challenge for the emerging applications of these plasma sources.

Plasma jets with a diameter of less than a millimetre are usually called microjets. The use of microjets is important to facilitate the processing of porous materials with fine grooves and holes. In 2002, Sankaran and Giapis have reported the characterization and application of hollow cathode sustained plasma microjets to deposit diamond crystals and poly-crystalline films using CH_4/H_2 mixtures as working gas [18]. Kim and co-workers have studied the effect of geometrical and operational parameters on controlling the microjet temperature and length [19]. In both of these studies, the length of the plasma channel was limited to the inter-electrode distance leading to limitations on processing space as well as device application. Kim has also studied a plasma source of single pin electrode configuration powered by either low- or radio-frequency with the helium gas feedstock and could produce microplasma jet length of 5-30 mm and 1.8-3.4 mm using, respectively, $kHz\,;800\text{-}1200\text{V}_{rms}$ and $RF\,;380\text{-}500\text{V}_{rms}$. In 2011, the possibility of guiding a pulsed microjet (of 2 mm diameter) with the repetition rate of 50 kHz in a flexible silicone tube have been reported by Clement and colleagues [20,21]. They could transfer the plume with maximum excited species toward downstream regions for possible remote treatment of biological cells.

Numerous methods for atmospheric pressure plasma characterization have been prposed [22,23,24,25]. Most are based on optical emission or absorption [26]. As long as the discharge is in the continuous mode (occurs at frequencies larger than MHz), methods will give the correct values of plasma parameters. In the case of pulsed plasmas, only a few methods are enable of measuring plasma parameters in real-time [27,28]. Most methods will just give values averaged over the acquisition time. Some methods have a high spatial resolution, while many others will average the signal over the probed volume [29]. Most of the methods also require a deep understanding of the physical phenomena, so the interpretation of the measured signal is far from being trivial. This is a reason why they are not routinely used by researchers who work on the modification of materials' surface properties by plasmas but are not specialists in plasma physics. To this end, the users are looking for a simple, cheap, and reliable technique for the characterization of atmospheric-pressure plasmas. One such technique is optical emission spectroscopy (OES), which can give information on the presence of various species in the discharge. Of course, It goes without saying that at atmospheric pressures, because of the effects of opacity and self-absorption inside the plasma column, the interpretation of optical phenomena are still challenging.

Characterization of plasma parameters such as electron and/or ion temperatures and densities, and the existence and abundances of other species (radicals, atoms in metastable states) is an important issue in tailoring the plasma parameters for a typical application which can be done using spectroscopic methods including laser scattering, laser induced fluorescence and laser absorption and molecular beam mass spectrometry [3 ,3 ,3], as well as Langmuir probes [29], microwave and laser interferometers [3], and Thomson scattering [3]. The use of electrostatic probes specially Langmuir probes is one of the low-cost and acceptable methods for plasma characterization, in which a collector is inserted into plasma then the drawn currents at various applied biasing voltages are measured. The collector must be carefully designed (material, radius and length of probe tip) to minimize its perturbation on the plasma. For this reason, there is no universal interpretation for the current-voltage (I–V) curve therefore there are various theoretical works published on it [3 ,3 ,3 ,3]. However, in spite of all difficulties, it can provide information about the local parameters in an acceptable accuracy.

These probes draw DC current from the plasma which can also include fluctuations that affect the characteristic (I–V) curve. These fluctuations are clearly visible in current-voltage characteristic curve of plasmas with AC sources (kHz, RF and MW powers). The most widespread use of Langmuir probes at present is in the semiconductor industry, where RF sources are used to produce plasmas for etching and deposition well under atmospheric pressure. Because of the source frequency induced fluctuations, the use of a simple single probe in these plasmas results in incorrect electron temperatures [3]. There are several approaches proposed to prevent happening of this kind of error; a) using a filter and/or compensation circuits b) making use of a double Langmuir probe (DLP) instead of a single probe (SLP).

A double probe has an independent and floating nature and basically is not affected by plasma [4] and capable of measuring the plasma characteristics locally [36,38,4]. In this configuration one of the electrodes being biased relative to the second one, rather than to the ground. The theory of the DLP is similar to that of a single probe, except that the current is limited to the ion saturation current for both positive and negative bias voltages which can be considered as an advantage of the double probe. The electron current could be completely controlled by the ion saturation current so that probe would draw a very little amount of current without disturbing the whole plasma condition.

The best method to evaluate the plasma plume at atmospheric pressure is the use of spectroscopy, which provides more reliable data but unlike the double probe which measures the characteristics of plasma locally, the spectroscopic approach gives information over a large volume of plasma. In 2007, Srivastava [4] showed that the electron temperatures from the Langmuir probe exceeded those obtained from spectroscopy. However, there are also works such as the research of Sun and co-workers [4], in which the results of the double probe confirm the results of spectroscopy. In fact, arriving radiations from different points of the plasma plume interfere in the spectroscopy of a specific point, so to localize measurements with high spatial resolution, very complex optics are required. However in the measurement with the Langmuir probe, it is possible to evaluate the evolution of electron temperature and density at different points along the plasma column.

In this study, a RF-driven atmospheric pressure plasma jet is designed and constructed; then, the plasma microjet parameters are evaluated by double probe measurements. The measurements are performed at different gas flow rates by applying the different RF powers on four positions on the jet axis. The electron excitation temperature is, also, measured using optical emission spectroscopy and the result obtained is compared with the results obtained from the Langmuir probe.

2. Probe measurements

As mentioned above, using a double probe is the easiest way to diagnose RF generated plasmas. Research on the measurement of electron temperature also suggests the superiority of the double probe over the single probe with compensation component [40]. The relationship between the current and voltage of the double probe tips is as follows [4]:   4

$$I = I_{iS} \tanh(\frac{eV}{2k_B T_e}) \tag{1}$$

in which, $I, I_{iS}, V, T_e, e, k_B$ are the current of double probe circuit, ion saturation current in the double probe, Potential difference between the two tips of probe, electron temperature, electric charge of electron, and the Boltzmann constant, respectively.

There are several methods for extracting electron temperature from the double probe characteristic curve [4 ,4 ,4 ,4 ,4 ,5]. The four frequently used methods, among others, namely the direct fitting of the equation   (1), double slope, turning point or Dote, and cutting or intercept method have been chosen and used to interpret the experimental data in this research.

In direct fitting method, the equation
(1) is fitted directly on the experimental data for different ion saturation currents and electron temperatures. When the two probes are not exactly identical the obtained characteristics curve will not be symmetrical, therefore the parameters of a and x_0 are added to the above mentioned relationship as the coordinates of the turning point of the curve to cover asymmetric states as well. These coefficients do not affect the calculation of temperature and electron density, because the electron temperature and ion saturation current are calculated from c and b, respectively. Therefore the generalized double probe equation to fit on the experimental data can be given as:

$$y = a + b \tanh[c(x - x_0)] \quad .$$

x_0 can be interpreted as the potential difference caused by the asymmetric placement of the probe tips, which causes the asymmetry of the characteristic curve and causes the current to flow in the absence of any applied bias, thus causing the altitude of a. The parameters b and c denote the be interpreted as the ion saturation current and the electron temperature, respectively.

In the double slope method, two slopes are drawn on the characteristic curve of the probe, one slope at the point of inflection, located at the origin in Fig. 1, and another slope in the ion saturation current region. The intercept of the two slopes gives the ion saturation current (I_{is}). The electron temperature (T_e) can be derived from equation (1) as follows [45,5]:   1

$$T_e(eV) = \frac{I_{is}}{2}\left[(\frac{dI}{dV})_{V=0} \right]^{-1} \quad . \tag{2}$$

In addition, the horizontal distance between the intersection points of the two slopes on both sides of the characteristics curve (Fig. 1) is equal to $4k_B T_e$ and the electron temperature can be derived from it.

The turning point or Dote method, shown in Fig. 2, uses the slope of positive ion saturation current, S, the slope of the characteristic curve at its inflection point, $\left(dI_p / dV\right)_{V=V_{inf}}$, and the total ion saturation current, $\sum_k I_{pk}$, determined by intersection points of the ion saturation slopes with inflection point slope to drive the electron temperature [47]:

$$T_e(eV) = \frac{\sum_k |I_{pk}|}{4\left[(\frac{dI_p}{dV})_{V=V_{inf}} - 0.82\, S\right]} \tag{3}$$

This method results in a more accurate electron temperature than other methods, because in other methods, if the slope of the ion saturation zone is larger, it leads to incorrect estimation of the electron temperature.

In the cutting or intercept method, the electron temperature is obtained using [46]:

$$T_e(eV) = \frac{V_d^{(2)} - V_d^{(1)}}{\ln\left(\frac{F-1}{D-1}\right)} \tag{4}$$

where, $F = \sum i_p / i_e^{(1)}$, $D = \sum i_p / i_e^{(2)}$, and other related parameters are shown in Fig. 3. It is found that, the proximity of values $V_d^{(2)}$ and $V_d^{(1)}$ to the knees of the curve leads to a good agreement of T_e with that obtained by the other methods.

We have used these four methods to evaluate the electron temperature and compared the results, as well as, used their averaged value to evaluate the electron density, Debye length and plasma frequency.

The electron density can be measured from the ion saturation current and electron temperature using the following equation [38]:

$$I_{is} = 0.6 e A n \sqrt{\frac{k_B T_e}{m_i}} \tag{5}$$

where A and n, respectively, denote the tip surface area and plasma density at far away from the probe.

As discussed earlier probe measurements have several limitations based on its complicated theory. Particularly in the case of collisional plasma or in the presence of magnetic field, probe measurements need correction for getting meaningful results. Early theories of the Langmuir probe were generally based on low pressure discharges, which did not take into account the interactions between particles in the probe shell and assumed the potential of the plasma to be invariant. In 1950 Johnson and Malter [46] were studied a time-varying discharge using a dual probe. The first attempt in studying collisional plasmas were made to form in the late 1990s, but the first appropriate mathematical analysis in this case has been reported by Su and Lam [52] as well as Cohen [53]. Using numerical results, Cohen presented a model for the study of collisional plasma probe. In 2002, Talukder [54] used Cohen's results and presented a normalized formulation for a single probe in collisional plasma, which was also developed in 2010 by Saito [55] for a dual probe.

At atmospheric pressures, the plasma becomes highly collisional as the ion-neutral mean-free-path becomes smaller than the Debye length. Neglecting of collisional corrections in formulation will result in unrealistic electron temperatures. Based on numerical results and a normalized formulation for a dual probe, it has been shown that in collisional plasmas, the electron temperature can be obtained from the following equation [55]:

$$T_e(eV) = \frac{I_{iS}}{6.16}\left[\left(\frac{dI}{dV}\right)_{I=0}\right]^{-1} \quad . \tag{6}$$

Theoretically I_{iS} should be the same for both probes but in practice, the curve is not symmetric and the two probes have different values of ion saturation currents. Therefore, I_{iS} is taken as an average of the saturation currents of both tips.

In addition, how to place the probe inside the plasma jet has been investigated by Blair [5] and been shown that the two tips may be placed symmetrically about the jet axis, which has been obeyed in this study.

3. Experimental setup and plasma jet aspects

Choosing a tapered geometry for the outer grounded electrode, an atmospheric-pressure plasma microjet ($APP\mu J$) device is designed and fabricated for further investigation on it. The system is designed such that the replacement of its parts to be very easy. The inner electrode, which could be a hollow cylindrical tube with different inner and outer diameters (here, a medical syringe) or solid steel nail rod with the same diameter as the outer diameter of the used syringes, is powered using a built in BNC-connector and RG-213U coaxial cable ($1.2\,m$ in length) via the RF L-type matching unit. The outer grounded electrode is shaved from aluminium in tapered shape so that the electrode thickness is $1\,mm$ all over it. The isolating dielectric (here Polytetrafluoroethylene (PTFE)) between the two electrodes is shaped the same as the outer electrode and placed inside of it to cover its inner surface. This system may be put, globally, into DBD-like plasma jet category proposed by Lu and co-workers in 2012 [5]. The working gas entrance is designed so that the gas could be injected straight along the radial direction as well as with a vortex type motion with a possible maximum angular velocity as shown in Fig. 4b. The working gas in this study was argon with the purity of 99.999% and various flow rates.

The dimensions of the constructed prototype are $38mm \times 15mm$ which can be made even smaller using sophisticated manners. The schematic of the constructed $APP\mu J$ and its gas injection structure together with an image of experimental setup showing the plasma jet together with the data acquisition system including a spectrometer (on the top of the image), dual Langmuir probe on a linear reciprocating system with a DC motor (from the front view), and a dielectric probe, on the right side of the image, (the results of which are not presented in this article) are shown in Fig. 4.

Several experiments were carried out by changing the type, shape, length, and diameter of the inner powered electrode. In all of these experiments, the inner electrode is powered by RF power generator ($Basafan\ RFG03BF$) with maximum output power of $300W$ and frequency of $13.56\,MHz$ as shown schematically in Fig. 4a. The measurements were carried in our laboratory where a relative humidity of 40% and a room temperature of $27\,°C$ are typical.

The electrical properties of the discharge were studied by measuring the voltage applied on the powered electrode and discharge current. The discharge currents are obtained by measuring the potential deference between the two electrodes of a $3.3nF$ capacity placed between grounded electrode and the ground. The data are registered by a $300\,MHz$ digital oscilloscope ($GW\ Instek\ GDS-2304A$) with a sampling rate bandwidth of $2\,GS/s$ and averaging over 256 samples, through a high voltage probe ($Pintek\ HVP-39Pro$). Fig. 5a shows typical variations of the discharge voltages and currents versus time.

In the plasma off mode, the phase difference between the current and voltage is nearly $90°$. In this case, there is a capacitive impedance of about M corresponding to the capacitance of $1.8\text{-}2.0\,pF$. The capacitance of the system in this state is measured using the RLC meter (KDK Kokuyo Electric Co. Ltd.: KC-605) to be $1.8\,pF$. On the other hand, when plasma is ignited, the phase difference between the voltage and the current reduces significantly. The current signal increases and deforms, while the peak-to-peak value for the voltage get smaller than for the plasma off state with no Ar gas flow. The plasma ignition introduces a parallel nonlinear load onto the electrical circuit and the slope of the $V-I$ curve is lower in this case (Fig. 5b).

If we consider the voltage to current (peak-to-peak) ratio as a measure of the real resistance (differential resistance) of the plasma system then according to Fig. 5b, the resistance of gaseous medium (before discharge ignition) is larger compared to its value for plasma (after ignition). In launched plasma jet, the increment of voltage lead to an increase in jet length, which can be related to increase in conductivity of the medium or decrease in its resistance as is discussed above.

4. The probe diagnosing

A double cylindrical Langmuir probe (DLP) was designed and constructed using a $0.3\,mm$ diameter tungsten wire. The probe tips with lengths of $1.5\,mm$ are located at the distance of $1\,mm$ from each other (Fig. 6). To find a typical dimeter of the possible launched plasma jet a series of scan experiments using various gas flow rates and applied RF powers was done which indicated the distance between the two probe tips should be less than approximately $1.2\,mm$ and has been taken into account in DLP design and construction.

High pressure plasmas are highly collisional environments and the collisions can prevent the formation of a suitable sheath in high gas flow rates and applied powers, sparking occurs between the tips of the Langmuir probe and causes corrosion of the tips and changes the characteristic curve of the probe. Any change and deviation in the characteristic curve deviates the plasma parameters from their real values. In addition, increasing the presence time of the probe inside the plasma also causes sparking and intensification of tip corrosion. To avoid these problems, the time of placing the probe inside the plasma should be reduced. For this purpose, the Langmuir probe was placed on a linear servo motor and the frequency of its reciprocating movements (along the axis of the probe and perpendicular to the direction of the plasma plume propagation) was set to 20 Hz (Fig. 7). The data collection voltage had a saw-tooth waveform and its repetition frequency was chosen to be 1000 Hz so that approximately 48 data series could be taken during the stay time inside the plasma and the average of these 48 data series was used as the characteristic curve of the probe. In this case, the disturbance caused by the probe and sparking between the probe tips is reduced and the resulting data for the electron temperature seemed more reasonable. An example of direct fitting on the characteristic curve is shown in Fig. 8Fig. 9, which was recorded under the conditions of gas flow rate of $4.5\,slm$ and applied power of 26W at position 2.

The plasma number density and electron temperature were measured using DLP in the jet at different axial locations. Experiments were done for different argon flow rates ($3, 4.5, 6, 7$ and $8\,slm$) and RF powers ($14, 18, 22$ and $26\,W$) at the four axial positions of onset, mid, end and out of the jet which are, respectively, indexed with $1, 2, 3$ and 4 in Fig. 6. A typical probe characteristic curve at position 3 for $4.5\,slm$ gas flow rate and applied power of 26 watts is shown in Fig. 8.

All of the voltage and current data were recorded using $300\,MHz$ digital oscilloscope ($GW\,Instek\,GDS\text{-}2304A$) and interpreted using Origin-2017 software. As mentioned in the introduction section, four different methods of modified direct fitting, double slope, turning point or Dote, and cutting or intercept were used to analyse data and calculate the electron temperature. The averaged electron temperature is corrected for collision effects, as illustrated in equation (6), by dividing it to 3.08, then, the result is used to calculate density and other parameters. Because of the higher probability of corrosion due to arcing and hence temperature rising, especially at high applied powers, data logging at the position 1, (the closest to the nozzle exit), was operated at a higher reciprocating speed.

Fig. 9 shows the obtained electron temperatures, plasma densities and saturated currents in four positions on the jet axis ($1, 2, 3$ and 4) under different argon flow rates ($3, 4.5, 6, 7$ and $8 \, slm$) with $14 \, W$ applied RF power.

It can be seen from Fig. 9 that the electron temperature has a local maximum at the position 2 then goes to the local minimum at the position 3 and eventually increase a bit sharply moving toward the position 4. The low temperature observed at the position 1 (at the active zone outlet) may related to the back-pressure occurred inside the discharge chamber due to the small outlet hole. The discharge chamber is strongly collisional and the electron temperature is lower. In the nozzle outlet duct where ionized gas launches to the ambient air, the gas outlet speed increases due to the Bernoulli's effect. The gas passing through the jet's hole, experiences a pressure drop and cools. The electron temperature in mid of jet (position 2) is higher which can be thought of the true jet electron temperature, can be due to the increased electron free path because of lower plasma pressure between positions 1 and 2. The decrease of the electron temperature toward the position 3 can be related to the increase in the plasma pressure and the increment of electron neutral collisions [5] as well as radiative recombination losses of ions and electrons. The electron temperature increment toward the position 4 cannot have a physical interpretation. It may be due to the very low ion saturation current in this position and hence larger error in the measurements as well as directed plasma divergent motion at that region as a result of electric field line fringe in this region.

The reduction of the ion density along the jet axis, maybe, due to recombination of charged particles in plasma and penetration of electronegative gases such as oxygen and nitrogen molecules and atoms from ambient air into the jet [56].

The effect of gas flow rate on the electron temperature, ion density and saturation current along the plasma jet axis at the above mentioned four different locations are also illustrated in Fig. 9. It can be seen that the electron temperature, regardless of some fluctuations within the error bars, behaves in a similar manner for the first three positions, monotonically increasing by the increment of gas flow rate, but the results for the fourth position behaves differently. For all of the flow rates, the electron temperature at position 2 is higher than the positions 1 and 3, but at position 4 it is the highest.

Increasing the gas flow rate is equivalent to an increase in gas pressure inside the discharge chamber leading increment in gas velocity when going out of the outlet hole. As reported by Mariotti and co-worker, and Roy and Talukder [58,5], it is expected that the electron temperature decreases with the flow rate increment. However, our results shown in Fig. 9a disagrees with it, viz. the electron temperature increases with the flow rate increment. This kind of behaviour has been reported by Bolouki and co-worker [6]. They reported the local maximum and slight fluctuations in the electron temperature curve with respect to changes in gas flow rate. Ouyang and co-worker [6] also reported an increase in electron temperature due to changes in gas flow rate in microwave plasma. It can be said that due to the highly collisional nature of the plasma, it becomes strongly affected by convective forces, the flow structures, and turbulence. The gas flow rate directly affects the flow velocity and the Reynolds number. In gas flow rates above $2.5 \, slm$, the plasma plume is in the phase of laminar-to-turbulent transition. The turbulence may be responsible for this kind of behaviour.

One can see from Fig. 9b that the ion density decreases with the increment of gas flow rates which can be an evidence of low electron – ion collision rates, again, due to an increase in pressure drop in plum region and recombination loss of charged species.

Finally, four measurement are performed by different applied RF powers for fixed $4.5 \, slm$ gas flow rate at position 2. The results are shown in Fig. 10. It can be seen that the electron temperature

decreases with the power increment which is in agreement with Mariotti and Blair's works [56,58]. Increasing the power, the plasma envelope around the central powered electrode increases so that more of the powered electrode lengths covered by plasma, therefore the total surface area available for electron emission getting maximum. The field in the plasma volume is probably weakened due to longer field path and higher electron density, as a consequence, energy exchanged between the field and the charged particles is also weakened leading to lowering the electron temperature by power increment, observed in Fig. 10. It has been explained that, this would not drastically affect the ionization efficiency by electron collisions at high electron energies. Because the overall electron temperature is reduced but the ionization rate is increased by a larger source of electrons at the powered electrode surface leading to an increased ion density [49,58,62].

Swift and Schwar have reported that DLPs measure only the upper 14% of the electron energy distribution [63]. Thus, the high T_e values obtained here may only represent the high end tail of the distribution and the vast majority of the electrons are at much lower temperatures. There are no wall losses of charged particle in plasma jets; therefore electrons are lost primarily via recombination reactions with ions. At low powers where the plasma volume is significantly smaller, the low energy electrons are lost in recombination reaction, due to the preferential electron–ion recombination of low energy electrons, leaving the high energy electrons to be collected by the probe so the measured electron temperature has to be slightly high. At higher input powers, there is also increased ionization and a larger plasma volume which can spread the energy among more particles and hence reduce the average electron temperature.

To compare the data obtained from the Langmuir probe, with the applied power of $30W$ and the gas flow rate of $3slm$, the emission spectrum of the plasma jet was recorded from the middle of the plasma plume (position 2), using an Ocean Optics spectrometer model HR2000, and shown in Fig. 11. There are various interpretations of emission spectra presented in different articles such as the intensity ratios lines from neutral excited atoms or ions, Stark broadening, Doppler broadening, and Boltzmann plot of neutral atoms or Saha-Boltzmann plot of ions [64,65,66,67,68,69,70,71].

The basis of the calculation in the method of the two neutral argon lines (Ar I) intensity ratio [73] is the use of two levels with a large transition energy difference, which makes the electron temperature calculation completely dependent on the choice of the selected two levels, so , a range of electron temperatures are obtainable. For example, by choosing the two couple of lines of 703.06 and $912.21nm$ and 794.49 and $912.21nm$ from Fig. 11, the electron temperatures of $0.68eV$, and $1.91eV$ are obtained, respectively. In 2018, Melnikov [74] used the intensity ratios of three emission lines of $425.93, 451.07$ and $763.53nm$ to $811.53nm$ and reported that the average temperature obtained from these three ratios was consistent with the temperature obtained from the Langmuir double probe. Using this method, the electron temperature of the plasma plume in our investigation is evaluated to be 1.44 to $3.38eV$ with the average value of $1.58eV$. As one can see from the Fig. 9, the electron excitation temperature at the position **2** for $26W$ applied power and $3slm$ of gas flow rate, measured by DLP, is nearly $6eV$ which is four times of the electron temperature obtained by optical emission spectroscopy (OEM) viz. $1.58eV$. This result is in good agreement with the reports of Balcon and colleagues and Garamoon et al. [75,76] which deduced that the electron temperatures obtained by OEM is in agreement within 25% of that obtained using Langmuir probe.

5. Conclusions

An RF-driven atmospheric pressure plasma microjet, APPµJ, is designed and fabricated with a tapered grounded electrode, and the plasma parameters are evaluated by double probe (DLP) measurements. Four usual methods of modified direct fitting, double slope, turning point or Dote, and cutting or intercept are explained mathematically and used to interpret the experimental data. It has been shown that all of these methods give nearly the same results, then, the average value of the obtained electron temperature is used for plasma density, Debye length and plasma frequency evaluations.

For comparison the results obtained by Langmuir probe, the emission spectrum of the plasma jet was recorded from the middle of the plasma plume, using an Ocean Optics spectrometer model HR2000. Based on the method that Melnikov has adopted regarding the intensity ratio of the three lines of $425.93, 451.07$ and $763.53 nm$ to $811.53 nm$, the recorded spectrum data were analyzed and the averaged electron excitation temperature of the plasma is obtained as $1.58 eV$. It has been shown that this value of the electron temperature is within the 25% of that obtained using Langmuir probe.

The plasma number density and electron temperature were measured along the microjet at four different axial locations. The results have shown that moving away from the outlet nozzle, the electron temperature found local maximum and minimum at the middle of the plasma plume, then this result has been interpreted. The ion saturation current and density monotonically decreased away from the outlet nozzle.

Measurements carried out at different input powers and showed that the electron temperature decreased by the increment of applied power, then, this result has been justified. However, the plasma density and the saturated current increased monotonically versus input power.

Figures and Tables
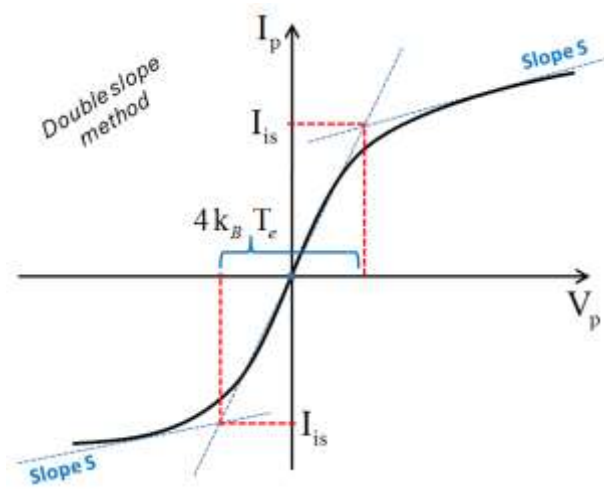
Fig. 1 Schematic diagram of the symmetric double probe characteristic to determine T_e in double slope method [45,47]
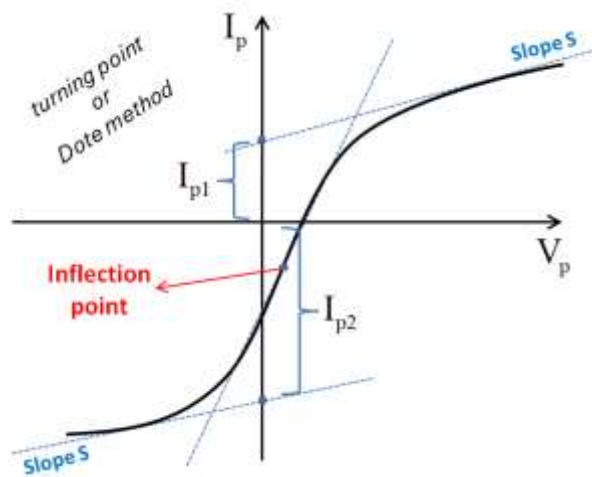
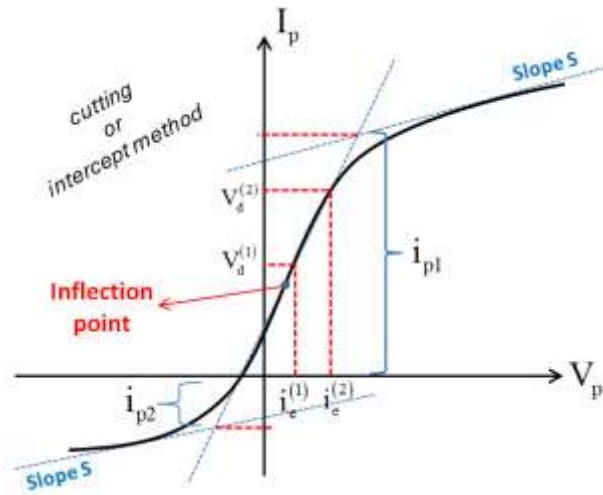Fig. 2) Schematic diagram of the double probe characteristic to determine T_e in turning point or Dote method [47]

Fig. 3) Schematic diagram of the cutting or intercept method to determine Te from the double probe characteristic curve [46]
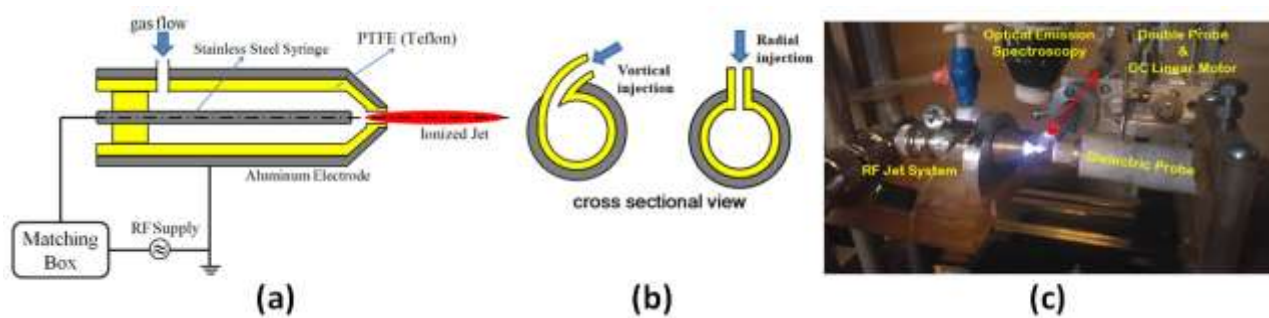
Fig. 4) a: Schematic of the designed atmospheric-pressure plasma microjet ($APP\mu J$), b: gas injection structure, c: an image of the plasma jet and together with the data acquisition system including a spectrometer on the top of the image, dual Langmuir probe on a linear reciprocating system with a DC motor (the front view), and a dielectric probe on the right side of the image (the results of which are not presented in this article).
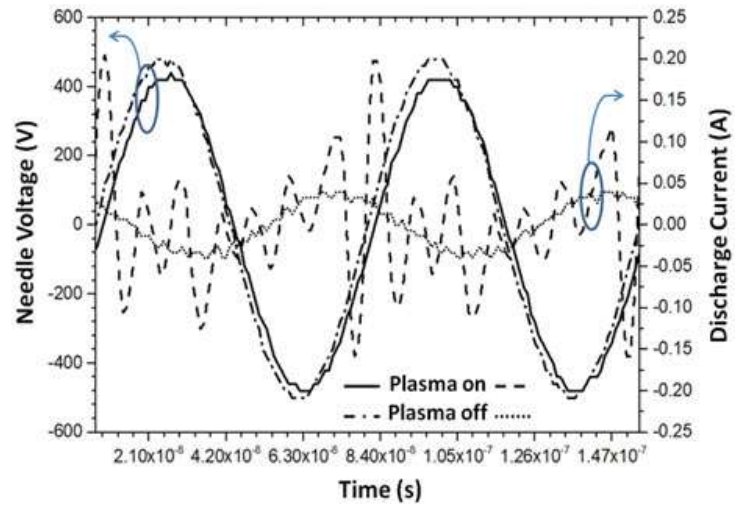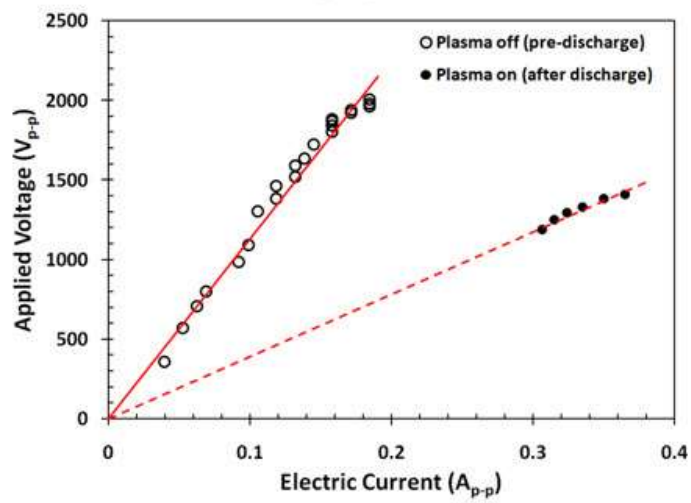
Fig. 5) Applied voltage with plasma on mode (solid) and without plasma off mode (dot-dashed) as well as discharge current measured with plasma on mode (dashed) and without plasma off mode (dotted) (a), V – I curve for plasma on/off (b).
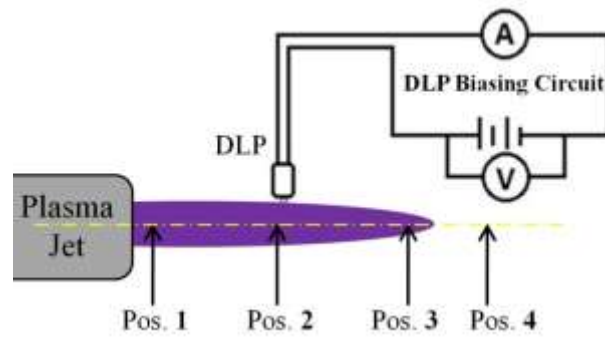
Fig. 6) A schematic of the testing layout. The voltage between the two probes from voltmeter can be detected and tuned. Also, the value of the probe current is read from the ammeter or oscilloscope.
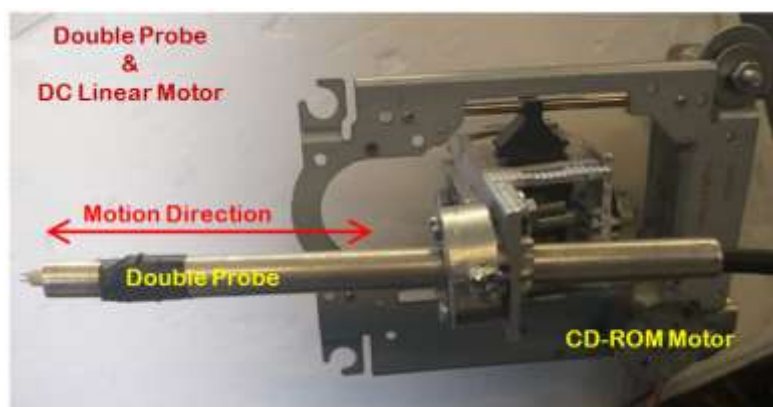
Fig. 7) Langmuir double probe on the linear reciprocating system which has been constructed using a CD-ROM DC motor.

Model	tanh (User)
Equation	y0+b*tanh(c*(x-x0))
Plot	Probe current
y0	-0.27127 ± 0.07305
b	25.28225 ± 0.08644
c	0.05247 ± 5.31405E-4
x0	-0.01985 ± 0.10191
Reduced Chi-Sqr	0.07804
R-Square(COD)	0.99983
Adj. R-Square	0.99961
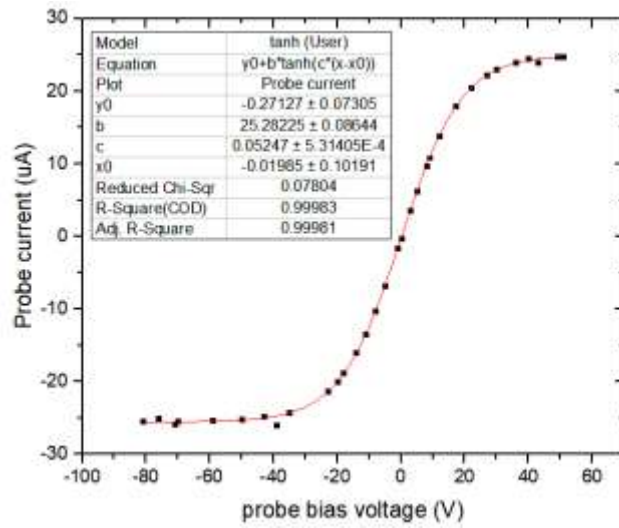
Fig. 8) A typical probe characteristic curve at position 2 by 4.5 slm gas flow rate and 26 watts applied power. Based on the direct fitting method, the hyperbolic tangent curve is fitted on the data and the electron temperature is calculated from the slope at the turning point of the curve (coefficient c).
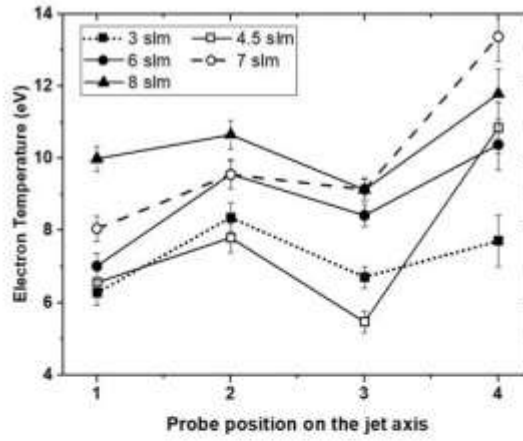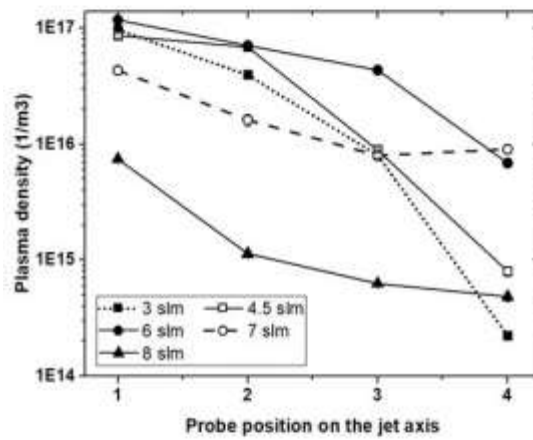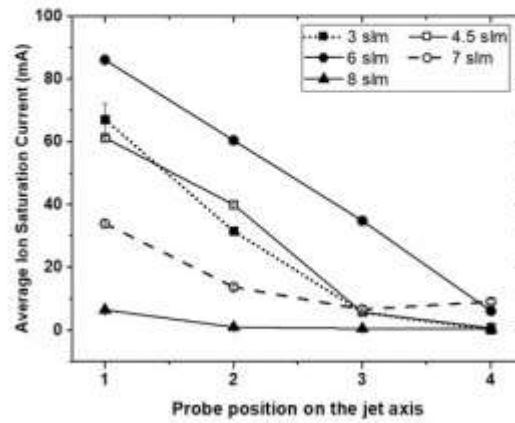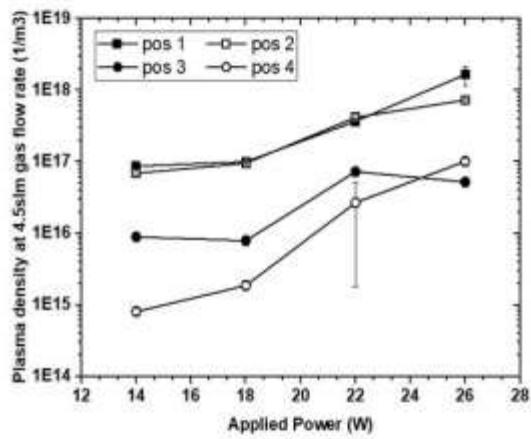
Fig. 9) The electron temperature (a), ion density (b) and the averaged ion saturation current (c), measured at four different positions of onset (1), middle (2), end (3) and outside the plasma jet (4) with a fixed $14W$ applied RF power.
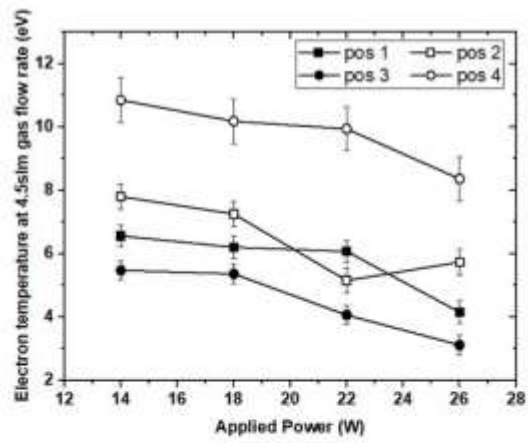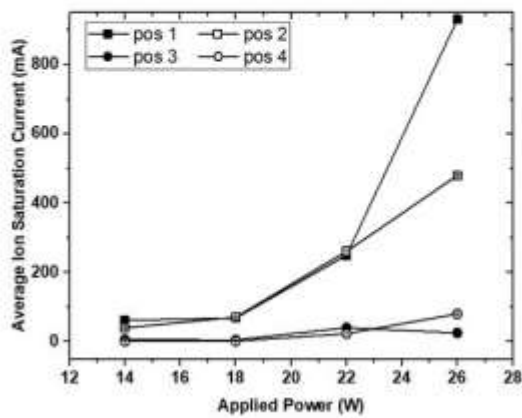
Fig. 10) The changes in electron temperature (a), ion density (b) and average ion saturation current (c) by increasing RF power. The RF power was set at $14, 18, 22$ and 26 W while the argon flow rate was constant at $4.5 \, slm$.

Fig. 11) Optical emission spectrum at middle of the plasma plume (position 2) with an applied power of 30 W and gas flow rate of $4.5\,slm$.

6. References

[1] C. Tendero, C. Tixier, P. Tristant, J. Desmaison and P. Leprince, Spectrochim. Acta B **61** (2006) 2–30

[2] M.G. Kong, G. Kroesen, G. Morfill, T. Nosenko, T. Shimizu, J. van Dijk and J.L. Zimmermann, New J. Phys. **11** (2009) 115012

[3] J. Laimer and H. Störi, Plasma Process. Polym. **4** (2007) 266–74

[4] T. von Woedtke, S. Reuter, K. Masur and K.D. Weltmann, Phys. Rep. **530** (2013) 291–320

[5] M. Vandamme, E. Robert, S. Lerondel, V. Sarron, D. Ries, S. Dozias, J. Sobilo, D. Gosset, C. Kieda, B. Legrain, J-M. Pouvesle, A. Le Pape, Int. J. Cancer **130** (2012) 2185–94

[6] J. Ehlbeck, U. Schnabel, M. Polak, J. Winter, T. von Woedtke, R. Brandenburg, T. von dem Hagen and K.D. Weltmann, J. Phys. D: Appl. Phys. **44** (2011) 013002

[7] R. Tiede, J. Hirschberg, G. Daeschlein, T. von Woedtke, W. Vioel and S. Emmert, Contrib. Plasma Phys. **54** (2014) 118–30

[8] K.D. Weltmann, E. Kindel, T. von Woedtke, M. Hahnel, M. Stieber and R. Brandenburg, Pure Appl. Chem. **82** (2010) 1223-1237

[9] J. Lalor, L. Scally, P.J. Cullen, V. Milosavljevic, J. Vacuum Sci. Technol. A **36** (2018) 03E108

[10] A. Sobota, O. Guaitella and A. Rousseau, Plasma Sources Sci. Technol. **23** (2014) 025016

[11] W. Shou-Guo, L. Hai-Jiang, Y. Tian-Chun and Z. Ling-Li, Chinese Phys. **13** (2004) 190

[12] E. Martines, M. Zuin, R. Cavazzana, E. Gazza, G. Serianni, S. Spagnolo, M. Spolaore, A. Leonardi, V. Delgianni, P. Brun, M. Aragona, I. Castagliuolo, P. Brun, New J. Phys. **11** (2009) 115014

[13] D. Dobrynin, G. Fridman, G. Fridman, A. Fridman, New J. Phys. **11** (2009) 115020

[14] H.M. Joh, S.J. Kim, T.H. Chung and S.H. Leem, AIP Advances **3** (2013) 092128

[15] J. Winter, M. Dünnbier, A. Schmidt-Bleker, A. Meshchanov, S. Reuter, and K. D. Weltmann, J. Phys. D: Appl. Phys. **45**(38) (2012) 385201

[16] H. Nishiyama, H. Takana, S. Niikura, H. Shimizu, D. Furukawa, T. Nakajima, K. Katagiri, and Y. Nakano, IEEE Trans. Plasma Sci. **36**(4) (2008) 1328–1329

[17] A. Schutze, J.Y. Jeong, S.E. Babayan, P. Jaeyoung, G.S. Selwyn, R.F. Hicks, IEEE Trans. Plasma Sci. **26**(6) (1998) 1685–1694

[18] R.M. Sankaran, K.P. Giapis, J. Appl. Phys. **92**(5) (2002) 2406-2411.

[19] D.B. Kim, J.K. Rhee, S.Y. Moon, W. Choe, Appl. Phys. Lett. **89** (2006) 061502

[20] F. Clement, P. Svarnas, L. Marlin, A. Gkelios, B. Held, IEEE Trans. Plasma Sci. **39**(11) (2011) 2364–5

[21] A. Gkelios, P. Svarnas, F. Clement, N. Spyrou, IEEE Trans. Plasma Sci. **39**(11) (2011) 2296–7

[22] S. Reuter, J.S. Sousa, G.D. Stancu, J.-P. Hubertus van Helden, Plasma Sources Sci. Technol. **24** (2015) 054001

[23] R. Zaplotnik, M. Bišćan, N. Krstulović, D. Popović, S. Milošević, Plasma Sources Sci. Technol. **24** (2015) 054004

[24] M. Mozetič, A. Ricard, D. Babič, I. Poberaj, J. Levaton, V. Monna, U. Cvelbar, J. Vac. Sci. Technol. A **21** (2003) 369–374.

[25] X.P. Lu, S.Q. Wu, IEEE Trans. Plasma Sci. **41** (2013) 2313–2326.

[26] C.O. Laux, T.G. Spence, C.H. Kruger and R.N. Zare, Plasma Sources Sci. Technol. **12** (2003) 125–138

[27] J. Wang, X. Gao, G. Xu, W. Zhang, J. Chang, H. Liu, W. Gao, Q. Zang and T. Ming, Phys. Scr. **78** (2008) 035501

[28] S. Wang, A.E. Wendt, J.B. Boffard, C.C. Lin, S. Radovanov and H. Persing, J. Vac. Sci. Technol. A **31** (2013) 021303

[29] K.G. Xu, S.J. Doyle, J. Vac. Sci. Technol. A **34** (2016) 051301

[30] P. Bruggeman and R. Brandenburg, J. Phys. D: Appl. Phys. **46** (2013) 464001

[31] S. Iseni, S. Zhang, A.F.H. van Gessel, S. Hofmann, B.T.J. van Ham, S. Reuter, K.D. Weltmann and P.J. Bruggeman, New J. Phys. **16** (2014) 123001

[32] J. Winter, M. Dünnbier, A. Schmidt-Bleker, A. Meshchanov, S. Reuter and K.D. Weltmann, J. Phys. D: Appl. Phys. **45** (2012) 385201

[33] A.S. Wan, T. Barbee, R. Cauble, P. Celliers, L.B. Da Silva and J.C. Moreno, Phys. Rev. E **55**(5) (1997) 6293-6296.

[34] B. Seo, S. You, J. Kim, Jpn. J. Appl. Phys. **54**(8) (2015) 086102

[35] N. Hershkowitz, How Langmuir Probes Work, in "Plasma Diagnostics", Vol.1, ed. by O. Auciello and D.L. Flamm (Academic Press, Boston, **1989**), Chap. 3

[36] F.F. Chen, Lecture Notes on "Langmuir Probe Diagnostics", Mini-Course on Plasma Diagnostics, *IEEE-ICOPS meeting*, Jeju, Korea, June 5, **2003**

[37] F.F. Chen, Phys. Plasmas **8** (6) (2001) 3029

[38] R.L. Merlino, Am. J. Phys. **75**(12) (2007) 1078

[39] F.F. Chen, Lecture notes on Langmuir probe diagnostics, Mini-Course on Plasma Diagnostics, IEEE-ICOPS meeting, Jeju, Korea, June 5, 2003

[40] R.M. Castro, G.A. Cirino, P. Verdonck, H.S. Maciel, M. Massi, M.B. Pisani and R.D. Mansano, Contrib Plasma Phys **39** (1999) 235-246

[41] I.H. Hutchinson, "Principles of plasma diagnostics", 2nd Ed, Cambridge University Press, **2002**

[42] A.K. Srivastava, M.K. Garg, K.S.G. Prasad, V. Kumar, M.B. Chowdhuri and R. Prakash, IEEE Trans. Plasma Sci. **35** (2007) 1135–1142

[43] J. Sun, H. Cai, Y. Zheng, X. Zhu, X. Zhang, Y. Liu, X. Sun, Z. Chao and H. Yin, Proc. SPIE 12284, 2021 International Conference on Optical Instruments and Technology: IRMMW-THz Technologies and Applications, 1228402 (8 July 2022)

[44] S. Bhattarai, Am. J. Eng. and Appl. Sci. **10** (4), (2017) 882-889

[45] F.F. Chen, "Electric probe: plasma diagnostic techniques", Edited by Huddleston and Leonard, *Academic Press*, New York, **1965**

[46] O. Johnson, L. Malter; Phys. Rev. **80** (1950) 58.

[47] T. Dote, Japanese J. Appl. Phys. **7** (1968) 964-965.

[48] S.S. Pradhan and D.C. Jana, J. of Physical Sci. **10** (2006) 158-163.

4 M.Y. Naz, A. Ghaffar, N.U. Rehman, S. Naseer and M. Zakaullah, Process in electromagnetic research **114** (2011) 113 -128

5 T. Uckan, Rev. Sci. Instr. 58 (1987) 2260

5 M. Konuma, "Film deposition by plasma techniques", *Springer-Verlag*, Berlin, **1992**.

5 C.H. Su, S.H. Lam, Phys. Fluids **6** (1963) 1479

5 I.M. Cohen, Phys. Fluids **6** (1963) 1492

5 M.R. Talukder, D. Korzec, M. Kando, J. Appl. Phys. **91** (2002) 9529

5 S. Saito, M.A. Razzak, S. Takamura and M.R. Talukder, J. Appl. Phys. **107** (2010) 123306

5 L.M. Blair and K.G. Xu, proceeding of 46th AIAA Plasmadynamics and Lasers Conference, Dallas, TX (**2015**) 2805

5 X. Lu, M. Laroussi and V. Puech, Plasma Sources Sci. Technol. **21** (2012) 034005

5 D. Mariotti, Y. Shimizu, T. Sasaki and N. Koshizaki, J. Appl. Phys. **101** (2007) 013307

5 N.C. Roy, M.R. Talukder, J. Bangladesh Acad. Sci. **40** (1) (2016) 23-36

6 N. Bolouki, J-H. Hsieh, C. Li, Y-Z. Yang, Plasma **2** (3) (2019) 283-293

6 Z. Ouyang, V. Surla, T.S. Cho, D.N. Ruzic, IEEE Trans. Plasma Sci. **40** (2012) 3476–3481

6 C.K. Kim, Korean J. Chem. Eng. **21** (3) (2004) 746 -751

6 J.D.D. Swift and M.J.R. Schwar, "Electrical Probes for Plasma Diagnostics" (*American Elsevier*, New York, **1970**)

6 H. H. Ley, A. Yahaya, R.K. Raja Ibrahim, J. Science and Technol. 6 (1) (2014) 49-66

6 A. Qayyum, M. Ikram and M. Zakaullah, Int. J. Modern Phys. B **17** (14) (2003) 2749-2759

6 A.M. Daltrini, S.A. Moshkalev, M.J.R. Monteiro, and E. Besseler, J. Appl. Phys. **101** (2007) 073309

6 X.-M. Zhu, J.L. Walsh, W.-C. Chen and Y.-K. Pu, J. Phys. D: Appl. Phys. **45** (2012) 295201

6 T. Namihira, K. Yamamoto and S. Katsuki, IEEE Trans. Plasma Sci. **35** (2007) 614–618

6 Y. Wang, C. Li, J. Shi, X. Wu and H. Ding, Plasma Science and Technology **19** (11) (2017) 115403

7 H.B. Baniya, R.P. Guragain, B. Baniya and D.P. Subedi, Reviews of Adhesion and Adhesives **8** (2) (2020) S1-S14(14)

7 H. Zhang, Y. Wu, H. Sun, F. Yang, M. Rong, F. Jiang, C. Wang and W. Huang, Plasma Chemistry and Plasma Processing **39** (6) (2019)

7 K. Dzieraega and K. Musio, J. Quantitative Spectroscopy and Radiative Transfer **52** (6) (1994) 747-754

7 A. Qayyum, M. Ikram and M. Zakaullah, Int. J. Modern Phys. B **17** (14) (2003) 2749-2759

7 A.D. Melnikov, R.A. Usmanov, N.A. Vorona, A.V. Gavirkov, G.D. Liziakin, V.P. Smirnov and R.A. Timirkhanov, Phys. Atomic Nuclei. **81** (11) (2018) 1536-1540

7 N.Balcon, A. Aanesland and R. Boswell, Plasma Sources Sci. Technol. **16** (2007) 217-225

7 A.A. Garamoon, A. Samir, F.F. Elakshar, A. Nosair and E.F. Kotp, IEEE Trans. Plasma Sci. **35** (1) (2007) 1-6